Journal of Molecular Structure, 270 (1992) 301–324
Elsevier Science Publishers B.V., Amsterdam

Vibronic spectroscopy of jet-cooled hydrogen-bonded clusters*

M. Gerhards, B. Kimpfel, M. Pohl, M. Schmitt[1] and K. Kleinermanns

Institut für Physikalische Chemie und Elektrochemie, Lehrstuhl I, Heinrich-Heine-Universität Düsseldorf, W-4000 Düsseldorf 1 (Germany)

(Received 3 January 1992)

Abstract

Mass-selected, two-photon resonant ionisation spectra of supersonically cooled *p*-cresol · $(H_2O)_n$ and phenol · $(H_2O)_n$ are reported. Cluster spectra with one, two and three water molecules attached can be unambiguously assigned.

A monotonic shift of the electronic spectra with increasing cluster size is not observed here. The spectrum of *p*-cresol · $(H_2O)_1$, is red-shifted relative to the free *p*-cresol spectrum, while the *p*-cresol · $(H_2O)_{2,3}$ electronic origins are blue-shifted relative to *p*-cresol · $(H_2O)_1$ but still lie on the red side of the monomer. Simple, highest occupied molecular orbital–lowest unoccupied molecular orbital (HOMO–LUMO) considerations based on ab initio calculations show that this can be explained by the inductive effect exerted on the O-atom of *p*-cresol, which acts as proton donor and acceptor in the H-bonding. The blue shift of n–π^* transitions of H-bonded chromophores with carbonyl groups like $CH_2O \cdot (H_2O)_1$ can be explained similarly.

Vibrational spectra of supersonically cooled complexes of *p*-cresol with H_2O and CH_3OH were further analysed by dispersed fluorescence and stimulated emission, detected by two-colour ionisation dip. In *p*-cresol · $(H_2O)_1$, progressions of the intermolecular cluster stretch vibration and its combination bands with intramolecular cluster vibrations were observed with similar frequencies in the S_0 and S_1 states. In *p*-cresol · $(H_2O)_3$, further intense intermolecular bands arise, namely the hydrogen-bridge bending and torsion vibrations. This can be attributed to the lower symmetry of these clusters. Ab initio quantum chemical calculations show *p*-cresol · $(H_2O)_3$ to have a higher H-bond stretch frequency than *p*-cresol · $(H_2O)_1$, because its (unsymmetric) cyclic structure is more rigid.

A characteristic pattern of CH_3 torsional bands in *p*-cresol is observed with complex structures due to CH_3 torsion–overall rotation interaction. Although their appearance is similar, the spacing of the monomer and cluster lines is very different, giving direct information on cluster structures from the rotational constants and moment of inertia.

Correspondence to: Professor K. Kleinermanns, Institut für Physikalische Chemie und Elektrochemie, Lehrstuhl I, Heinrich-Heine-Universität Düsseldorf, W-4000 Düsseldorf 1, Germany.

* Dedicated to Professor N.D. Sokolov on the occasion of his 80th birthday.

[1] Present address: Physikalisch-chemisches Institut, Universität Heidelberg, D-6900 Heidelberg, Germany.

INTRODUCTION

Traditionally, the interaction of solvent molecules with a solute molecule has been studied spectroscopically, by monitoring changes in intramolecular bond properties by the spectral shifts in vibrational bands and changes in electronic surface positions by the shifts of the electronic spectra. Most experiments were performed in the liquid phase, but some occurred in the gas phase at room temperature. The broad linewidths here clutter the spectra and make interpretation on a molecular level difficult.

The supersonic expansion technique is a powerful tool for preparing isolated ultracold molecules with simplified spectra and a number of complex partners, depending on the expansion conditions. The electronic spectra show sharp, rotationally cooled lines suitable for the direct study of intermolecular (cluster) vibrations of a solvent–solute complex, even when their vibrational progressions show very small frequency differences.

Supersonically cooled spectra provide interesting insights into microscopic solvent–solute interactions and the process of solvation in general. This work concentrates on the study of *p*-cresol · (H_2O) H-bonding. *p*-Cresol is selected as a model molecule for two reasons. First, *p*-cresol is the chromophoric group of the amino acid tyrosine and thus suited to the study of H-bonding in amino acids and protein solvation. From its cluster spectra we may learn about the way the solvent molecule(s) surround(s) the solute molecule, i.e. the structure of different cluster conformations and the dynamics of both the solvated species and the complex. H-bonding plays an important role in stabilising the three-dimensional structure of proteins and protein–nucleotide complexes.

The *p*-cresol $(H_2O)_n$ spectra are very similar to the phenol $(H_2O)_n$ spectra which represent prototype H-bonded complexes of aromatic chromophores. In the cresol system we observe additional bands due to the internal rotation of the CH_3 group. From their typical pattern we learn about the way in which CH_3 rotation is hindered both in the monomer and in the complex. Some of the CH_3 torsion bands show interesting and complex structure due to torsion–overall rotation interaction. This structure looks quite different in the cluster.

For a better understanding of the spectra, ab initio calculations on the Hartree–Fock and second-order Møller–Plesset theory (MP2) level were performed to form a basis for intermolecular vibration and spectral-shift calculations. Detailed intermolecular potentials for the stretching, bending and torsional vibrations are obtained and compared with experimental data.

Simple HOMO–LUMO considerations show the shift of the electronic spectra in the π–π^*-transitions of the *p*-cresol · $(H_2O)_n$ — or phenol · $(H_2O)_n$ — system and in the n–π^*-transitions of H-bonded chromophores with

carbonyl groups like $CH_2O \cdot (H_2O)_1$ to be due to the inductive effect exerted on the O atom of the chromophores. The OH group acts as proton donor and acceptor in the cresol and the C=O group as acceptor in the case of formaldehyde.

EXPERIMENTAL

The experimental setup is similar to that described previously [1] and consists of a high vacuum apparatus, an electromagnetically pulsed, heatable injection valve (600 μs–1.2 ms gas pulse width, 0.15 mm nozzle hole) for skimmed jet expansion of *p*-cresol/H_2O/He, a differentially pumped time-of-flight (TOF) mass spectrometer, and an excimer laser (Lambda Physik EMG 100) pumped linear dye laser (FL 2002; 0.2 cm^{-1} FWHM) for work in the wavelength range 270–283 nm (using coumarin 153 dyes and FL 30 and FL 31 frequency-doubling crystals). Background pressures were 3×10^{-4} mbar, 10^{-5} mbar and 2×10^{-6} mbar (beam on) in the main chamber, the differentially pumped ionisation chamber, and the time-of-flight chamber, respectively. The vacuum was maintained by two 2600 l s^{-1} diffusion pumps (Edwards), backed by a roots/rotatory pump system (Alcatel) and a liquid nitrogen trap, and a 150 l s^{-1} turbopump (Leybold Heraeus Turbovac 3600) for the three chambers. The multiphoton ionisation (MPI) spectra were usually taken at 0.12 mbar *p*-cresol, 1–5 bar helium, 0.05 mbar H_2O, and a laser–nozzle probe distance $x/d = 500$. In some of the experiments the water concentration was varied by using a peltier element-driven cooler.

Time-of-flight spectra were obtained by averaging the preamplified ion signals from a microchannel plate detector (Galileo Chevron type) with a digital oscilloscope (Le Croy model 9400). The mass resolution is 90 at $m/e = 108$. Some spectra were taken with a home-built reflectron type TOF-mass spectrometer with resolution 800 at $m/e = 108$. Resonance enhanced multiphoton ionisation (REMPI) spectra were recorded by integrating the ion signal within a certain TOF-interval (mass) with a gated boxcar (Stanford Research SR 250). Laser, nozzle, and boxcar were synchronised by a four-channel digital delay/pulse generator (Stanford Research DG 535).

For the dispersed fluorescence measurements, the pump light was fixed to a selected vibronic level and the fluorescence was dispersed by a 30 cm monochromator (McPherson 218) in the first order. The dispersed light was detected by a cooled photomultiplier (Thorn EMI 9789 QB; – 30°C) and the photocurrent was averaged by a gated boxcar (Stanford Research SR 250) and recorded by a chart recorder.

For the dump process in the two-colour ionisation dip experiments, another excimer laser (Lambda Physik EMG 200) pumped dye laser (Lambda Physik FL 2002) was used with the frequency-doubled output of

coumarin 153, rhodamine 6G and sulphorhodamine B dyes, depending on the wavelength range to be covered. The two laser beams were aligned coaxially with beam diameters of around 1.5 mm and triggered to have zero time delay (jitter around ± 5 ns). The intensity of the pump light ω_1 was weakened to avoid the resonant multiphoton ionisation caused by ω_1 alone. Under these conditions, spatial and temporal overlap of pump and dump beams could be easily aligned by optimising the large two-colour ionisation signal. The ions produced were drawn to the detector (Cu–Be multiplier) by its electric field and the ion current was averaged by the boxcar system described above.

RESULTS AND DISCUSSION

Cluster size assignment

An unambiguous assignment of cluster size is one of the most important problems in cluster jet spectroscopy.

A very elegant approach is to use elastic scattering to kinematically preselect clusters of specific size [2]. Very high-resolution rotational spectra in many cases also lead to a correct cluster size assignment from the precisely measured moments of inertia of the clusters [3]. Mass-resolved resonant ionisation spectra with "soft" excitation just above the ionisation threshold avoids or reduces fragmentation of the mother ion and therefore allows size assignment from mass information. Especially for the fragile larger H-bonded clusters, even soft two-colour ionisation may lead to fragmentation if the vertical ionisation energy is well above the adiabatic limit, due to large potential energy shifts of the neutral and ion cluster. Excitation of cluster ion vibrations may lead to fragmentation obscuring the size assignment.

Attempts have been made to perform cluster size assignments by measurement of cluster densities as a function of solvent and inert gas stagnation pressures and to compare these measurements with the corresponding approximate analytical solutions. A more general approach, able to extract rate coefficients for cluster formation, is the numerical integration of the differential rate equation system describing the density evaluation as a function of chemical clustering and volume expansion in the jet. The full cluster density evaluation as a function of solvent concentration indeed allows a clear size assignment, at least for smaller clusters, even in the absence of mass information [4].

Figure 1 shows the two-photon ionisation spectra of *p*-cresol · $(H_2O)_n$ (n = 0–3) after S_0–S_1 (π–π^*) excitation, as measured by tuning the boxcar gate to the time-of-flight (mass number) of the individual clusters. Figure 1(a) shows the REMPI spectrum of free *p*-cresol (m/e = 108) seeded in 4 bar of

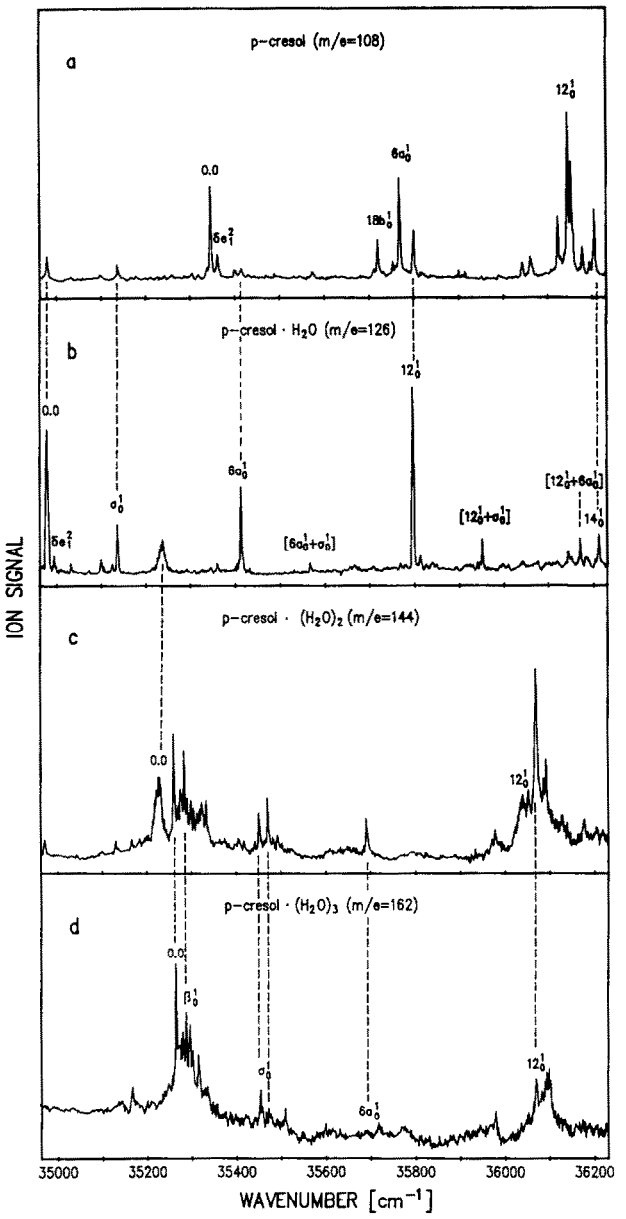

Fig. 1. Mass-selected REMPI spectra of *p*-cresol · $(H_2O)_{0,1,2,3}$ from excitation of the $S_0 \rightarrow S_1$ transition. (a) Free *p*-cresol; (b) *p*-cresol · $(H_2O)_1$; (c) *p*-cresol · $(H_2O)_2$; (d) *p*-cresol · $(H_2O)_3$. Corresponding vibronic bands are connected by (– – –), indicating a general fragmentation behaviour of *p*-cresol · $(H_2O)_n \rightarrow$ *p*-cresol · $(H_2O)_{n-1}$. Experimental conditions are 4 bar helium, *p*-cresol 1 Torr and expansion distance $x/d = 500$.

helium between 35 000 and 36 200 cm^{-1}. The band at 35 337 cm^{-1} is the lowest frequency band of bare *p*-cresol and can be assigned to the electronic origin 0,0 (free). The bands at 35 337 + 419 and + 803 cm^{-1} can be assigned to the totally symmetric $a_1(S_1)$ state fundamental vibrations 6a and 12 which are localised mainly in the aromatic ring. The weaker feature at 370 cm^{-1} is the 18b skeletal vibration with b_2 symmetry. The very weak low-frequency bands in Fig. 1(a) arise from fragmentation of *p*-cresol · $(H_2O)_1$ (6a) and mainly from the hindered internal rotation of the CH_3 group of *p*-cresol, which is analysed below. The bands generally show efficient rotational cooling with rotational temperatures < 2 K.

Figure 1(b) shows the REMPI spectrum of *p*-cresol · $(H_2O)_1$ at mass number 126 (108 + 18). The electronic origin 0,0 of the monohydrated *p*-cresol is located at 34 980 cm^{-1} with a red shift of 357 cm^{-1} relative to bare *p*-cresol. From the complex origin, a vibrational progression starts with a frequency interval of 152 cm^{-1}. From the isotopic shift of the corresponding band in $C_7H_7OD \cdot D_2O$ and from comparison with ab initio SCF calculations of the cluster potential along the OH ··· O-coordinate (see next section D), we can assign this transition to the intermolecular stretch vibration.

Further bands arise from the intramolecular $a_1(S_1)$ cluster transitions 6a and 12 as well as from combinations of σ with intramolecular cluster vibrations. Figures 1(c) and (d) show that the 0,0 bands of *p*-cresol · $(H_2O)_{2,3}$ are blue-shifted from the origin of *p*-cresol · $(H_2O)_1$ by 250 cm^{-1} and 287 cm^{-1} respectively. Figure 1 shows a distinct fragmentation of *p*-cresol · $(H_2O)_n$ to *p*-cresol · $(H_2O)_{n-1}$. Corresponding vibronic bands are connected by dashed lines in Fig. 1, demonstrating this fragmentation behaviour. No fragmentation to *p*-cresol · $(H_2O)_{n-2}$ could be detected. This fragmentation behaviour is not limited to the 0,0 bands, but is also found after excitation of higher energy vibronic bands, as Fig. 1 shows. The simple fragmentation behaviour allows unambiguous cluster size assignment for $n = 1$–3. According to this assignment the *p*-cresol · $(H_2O)_1$ spectrum is considerably red-shifted relative to free *p*-cresol and shows a number of intermolecular and intramolecular vibronic bands. The spectrum of *p*-cresol · $(H_2O)_2$ is blue-shifted relative to *p*-cresol · $(H_2O)_1$ and shows broad bands, namely the 0,0 and the 12 bands in Fig. 1(c). The *p*-cresol · $(H_2O)_3$ spectrum is even further blue-shifted but still lies at longer wavelengths than free *p*-cresol. It again shows sharp peaks with a great number of low-frequency intermolecular bands, as well as intramolecular aromatic ring vibrations which are analysed below.

The higher energy vibronic bands of *p*-cresol · $(H_2O)_3$ fragment very easily and show more intense peaks at $n = 2$ than at $n = 3$.

Figure 2(b) shows the dependence of *p*-cresol–H_2O cluster formation on H_2O concentration at an expansion distance $x/D = 40$ ($x = 20$ mm;

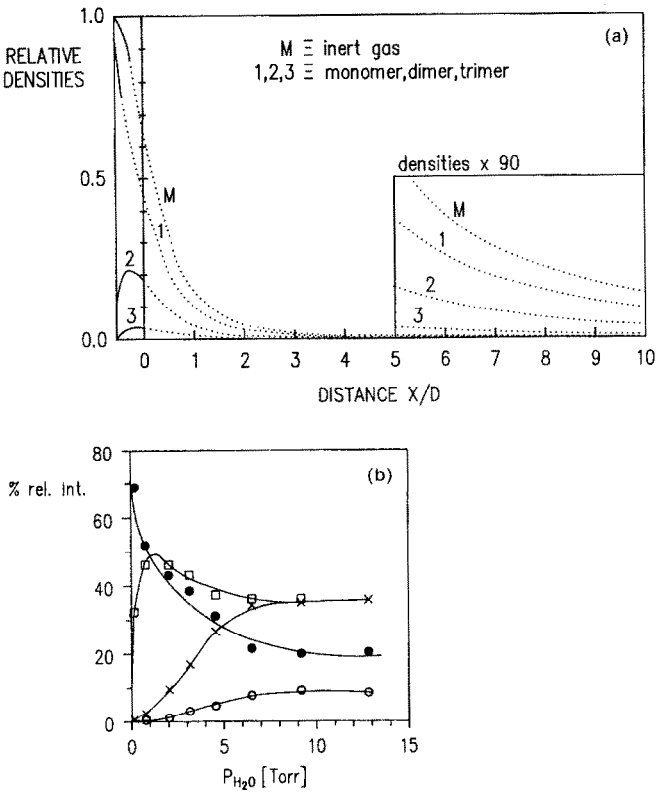

Fig. 2. (a) Calculated cluster self-association along the expansion axis of the supersonic jet. Conditions are 1 bar inert gas M, 20 mbar solvent, $k_1 = k_2 = k_3 \times 10^{-33}\,cm^6\,s^{-1}\,particles^{-2}$, $k_{n,n+1} = 0$ and 1, 2 or 3 is cluster size n. The range of integration extends from $x/d = -0.6$ to $x/d = 10$. The integration had to be started at negative x/d because the Mach number is already greater than zero at $x/d > -0.6$. The strong increase in cluster density in the range $-0.6 \leqslant x/d \leqslant 0$ is clearly due to neglecting reverse reactions, which is a better approximation at low temperatures and densities, i.e. at greater expansion distances. (b) Dependence of *p*-cresol/H_2O cluster formation on H_2O concentration at an expansion distance $x/d = 40$, [He] = 4 bar, [*p*-cr] = 0.2 Torr. Change in the fluoresence intensity of the *p*-cresol/H_2O cluster electronic origins 0,0 with H_2O concentration. (●) origin of free *p*-cresol at 35 337 cm^{-1}; (□) origin of *p*-cresol · $(H_2O)_1$ at 34 980 cm^{-1}; (x) origin of *p*-cresol · $(H_2O)_2$ at 35 230 cm^{-1}; (○) origin of *p*-cresol · $(H_2O)_3$ at 35 261 cm^{-1}. The lines show the corresponding calculated change of relative cluster concentration with H_2O concentration at the experimental expansion distance $x/d = 40$.

$D = 500\,\mu m$). We observe typical behaviour for cluster association by consecutive reactions. The monomer curve (●) decreases nearly exponentially with increasing H_2O concentration due to consecutive H-bonding and cluster formation. The *p*-cresol · $(H_2O)_1$ curve (□) assigned from mass analysis initially rises fast and decreases again at higher H_2O concentration due to formation of higher clusters $n > 1$. The $n = 2$ (x) and $n = 3$ (○)

curves rise much more slowly and obviously at the expense of the $n = 1$ concentration.

Figure 2(a) shows typical cluster densities as a function of the expansion distance obtained from numerical integration of the rate-equation system after transformation of the density change from time to expansion distance. From the corresponding curves for solvent–solute formation calculated for different solvent concentrations, one obtains the cresol · $(H_2O)_n$ cluster densities at the experimental expansion distance as a function of H_2O pressure (lines in Fig. 2(b)). The numerical integration is based on the most simple scheme of successive cluster formation

$$\begin{aligned}
&H_2O + H_2O + He \xrightarrow{k_1} (H_2O)_2 + He \\
&p\text{-cr} + H_2O + He \xrightarrow{k_2} p\text{-cr}(H_2O)_1 + He \\
&p\text{-cr}(H_2O)_1 + H_2O + He \xrightarrow{k_3} p\text{-cr}(H_2O)_2 + He \\
&p\text{-cr}(H_2O)_2 + H_2O + He \xrightarrow{k_4} p\text{-cr}(H_2O)_3 + He.
\end{aligned} \tag{1}$$

The decrease of H_2O concentration by self-association is simplified and considered as dimerisation. Reverse reactions and temperature dependence of the rate constants were not taken into account. By fitting the four rate constants, nearly perfect agreement between experiment and theory was obtained. In particular, no reasonable set of rate constants could be obtained with a different cluster size assignment, i.e. $n = 1$ and 2 or $n = 2$ and 3, exchanged. The $n = 0$–3 assignment from the fit of the full kinetic curves is unambiguous. The four rate constants were varied in the range 10^{-30}–$10^{-35}\,cm^6\,s^{-1}$ $(particles)^{-2}$. The best fit is [4]

$$k_1 = 6 \times 10^{-32}\,cm^6\,s^{-1}$$

$$k_2 = 6 \times 10^{-32}\,cm^6\,s^{-1}$$

$$k_3 = 3.5 \times 10^{-32}\,cm^6\,s^{-1}$$

$$k_4 = 1.5 \times 10^{-32}\,cm^6\,s^{-1}.$$

with error limits of $\pm 30\%$ as guessed from their sensitivity to fit the experimental data. Obviously the strongly simplified kinetic scheme (1) limits the accuracy of the rate constants. In spite of this, the decrease of the rate coefficients with increasing cluster size seems real to us. One may speculate that this order correlates well with the decrease of H-bond strengths obtained in the ab initio calculations (see below) for *p*-cresol acting as proton donor and acceptor respectively in *p*-cresol · $(H_2O)_{1,2}$ and with the low entropy of the presumably cyclic *p*-cresol · $(H_2O)_3$.

In summary, cluster size assignments from the mass information of resonant (1 + 1)-MPI experiments and from the full kinetic curves of

cluster density as a function of solvent concentration are in full agreement. The kinetic approach to size assignment may also be valuable for other spectroscopic methods like coherent antistokes Raman scattering (CARS) or laser induced fluorescence (LIF) which inherently do not possess mass information. Admittedly, the measurement of the full kinetic curves shown in Fig. 2(b) is quite cumbersome when performed for a number of spectral bands. However, the cluster size assignment obtained from the comparison with kinetic simulation (and sometimes even from simply looking at the curve) is unambiguous and straightforward, at least for the smaller clusters.

Simple perturbation treatment of the spectral shifts on the HOMO–LUMO level

Once a correct cluster size assignment has been obtained, the detailed spectral features can be investigated to obtain information on cluster structures by comparison with theory.

Ab initio calculations on the Hartree–Fock level were performed on the structures of *p*-cresol · $(H_2O)_{0-3}$. We used the GAUSSIAN 80 program for calculation on an IBM 3090. Due to the size of the molecular systems, the restricted Hartree–Fock calculations could be performed only with the minimal STO-3G basis set, which restrict the quantitative meaning of the results.

By extensive geometry optimisation, we obtained the cluster configurations of *p*-cresol · $(H_2O)_n$ (n = 0–3) shown schematically in Fig. 3. In the first association step, the water molecule acts as proton acceptor. The H-bonding lies in the plane defined by the benzene ring, while the plane of the water molecules orients perpendicular to the ring. This configuration is called translinear.

In the second association step, it is energetically more favourable for the water molecule to act as proton donor and thus form a hydrogen bond to the O-atom of the cresol OH group, than to cluster with the first water molecule. In the most stable configuration of *p*-cresol · $(H_2O)_3$, the third water molecule associates with the second and acts as proton donor, forming an "open cyclic", non-planar solvent ring. We obtain H-bond energies [5]

$$\Delta E_n = E(n) - [E(n-1) + E(H_2O)]$$

of -32.0, -23.4 and $-32.3\,\mathrm{kJ\,mol^{-1}}$ for n = 1–3

The higher solvation energy of the first association step as compared to the second can be explained by the considerable acidity of free *p*-cresol, favouring proton-donor behaviour. The high H-bond energy of the third association step, however, necessitates a second, weaker H-bond which the

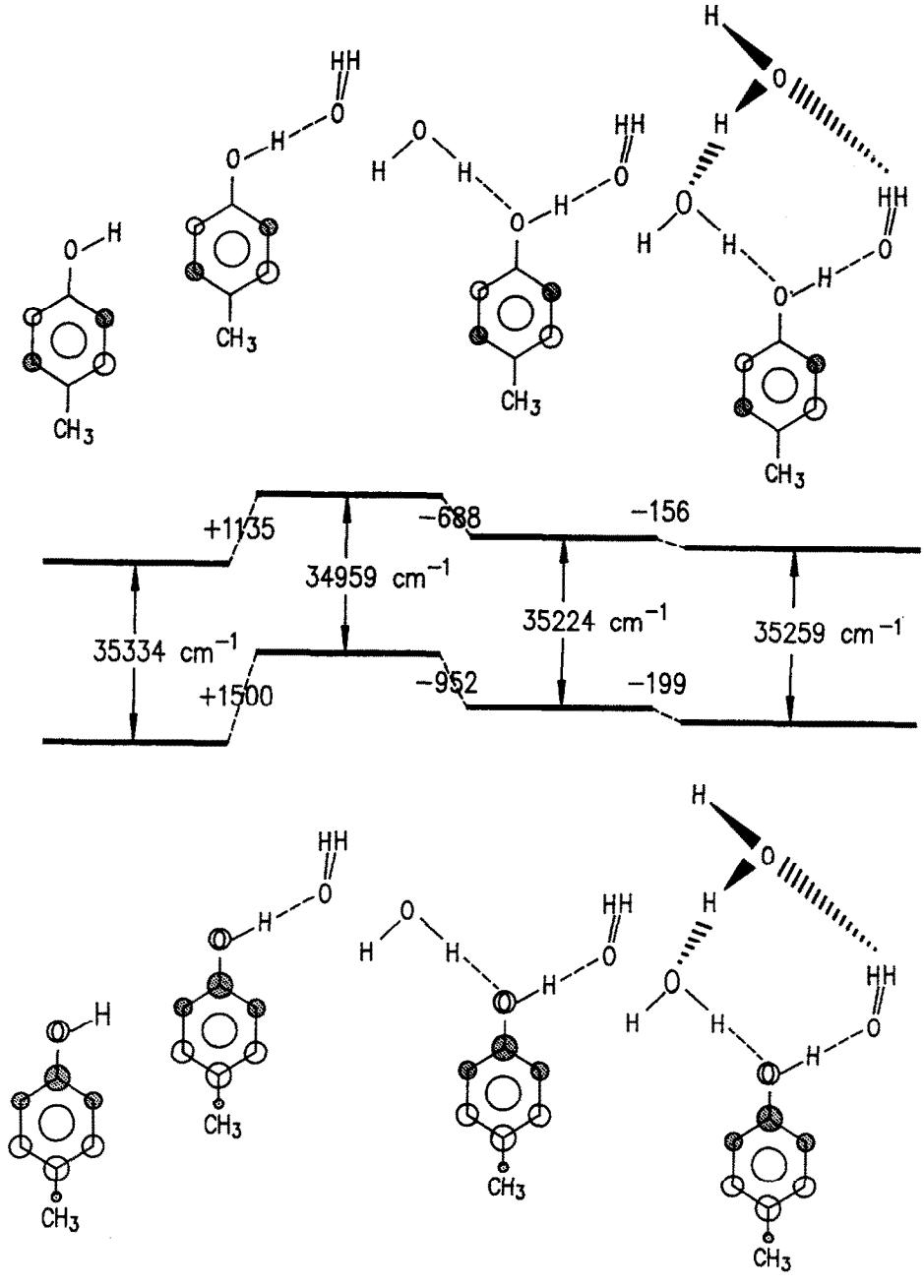

Fig. 3. HOMO/LUMO energetics and MO coefficients in free *p*-cresol and $(H_2O)_{1,2,3}$ clusters. The optimised cluster structures are also shown.

TABLE 1

Spectral position of the electronic origins of *p*-cresol (solvent) according to experiment and ab initio GAUSSIAN 80 calculations (STO-3G basis sets)

Species	ν_{exp} (cm^{-1})	$\Delta\nu_{exp}$ (cm^{-1})	$\Delta\nu_{calc}$ (cm^{-1})
p-cresol	35 337	0	0
p-cresol · $(H_2O)_1$	34 980	−357	−375
p-cresol · $(H_2O)_2$	35 230	−107	−110
p-cresol · $(H_2O)_3$	35 261	−76	−72

unsymmetric and non-planar cyclic solvent structure in Fig. 3 indeed shows.

In addition to the total energy of an energetically optimised cluster geometry, the Hartree–Fock procedure also yields the eigenvalues of the one-electron molecular orbitals. The electronic origin of the cluster $S_0 \rightarrow S_1$ excitation, can be considered as arising from the transition of an electron from the HOMO to the LUMO. Although not even approximate absolute transition energies can be expected from this single-determinant, minimal basis set procedure, the HOMO–LUMO energy differences describe relative spectral shifts in a "homologous row" of solvent association steps very well. The spectral shifts in Table 1 show nearly quantitative agreement between experiment and theory with the (0, 0)-transition frequency of free *p*-cresol as the only fit parameter. Only the cluster structures described with *p*-cresol acting as proton donor and acceptor in *p*-cresol · $(H_2O)_{1,2}$ respectively and an "open cyclic" arrangement for *p*-cresol · $(H_2O)_3$ yield this satisfactory agreement. Complete neglect of differential overlap/configuration interaction (CNDO/CI) calculations showed even the absolute transition energies to be correct within $\approx 10\%$ for the cluster structures shown in Fig. 3.

Considering the longest wavelength excitation of *p*-cresol and its clusters with water to arise from a HOMO–LUMO transition in molecular orbital language, we can look more closely at the physical reasons for the observed spectral shifts in Fig. 3. We see that both HOMO and LUMO of the π system are destabilised after addition of the first water molecule, which acts as proton acceptor, while they are stabilised again after addition of the second and third water molecules, which act as proton donors. It is now well known from simple Hückel theory that electron-donating substituents or solvents exert a $+I$ effect and destabilise the π system while $-I$ substituents stabilise it in agreement with Fig. 3. More quantitatively, in terms of first-order perturbation theory, the change in π-system energy of the ground and excited states due to an inductive effect on some centre (here

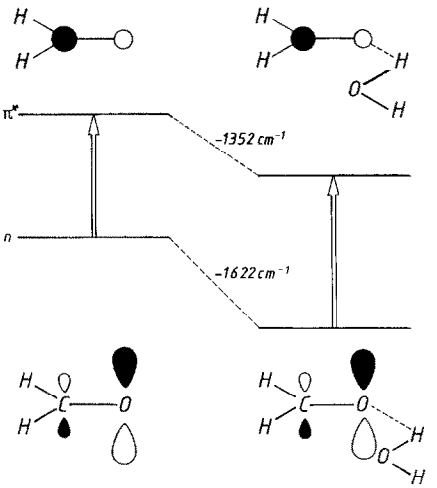

Fig. 4. HOMO/LUMO energetics and MO coefficients in CH_2O and $CH_2O(H_2O)$ according to ab initio gaussian calculations with the 6-31G** basis set. The optimised structure is also shown.

the O-atom of cresol) is

$$\delta E_\pi = q_0 \delta\alpha_0$$
$$\delta E_\pi^* = q_0^* \delta\alpha_0 \tag{2}$$

with q_0 and q_0^* as O-atom charge order defined by: $\Sigma\, b_j C_{j0}^2$ (b_j, population number; C_{j0}, O-atom orbital coefficient in the jth MO); $\delta\alpha_0$ as change in the Coulomb integral at the oxygen atom which is positive (destabilising) for $+I$ solvent effects and negative (stabilising) for $-I$ solvent effects.

The microscopic shift after addition of the solvent is

$$\begin{aligned}\Delta\delta E_\pi &= \delta E_\pi^* - \delta E_\pi \\ &= (q_0^* - q_0)\delta\alpha_0 \\ &= (C_{LO}^2 - C_{HO}^2)\delta\alpha_0\end{aligned} \tag{3}$$

TABLE 2

H-bond energies (kJ mol^{-1}) of $(H_2O)_1$-clusters for different basis sets

Cluster	Basis set		
	4-31G*	6-31G*	6-31G**
$CH_2O \cdot (H_2O)_1$	−22.58	−21.28	−21.63
$CH_3CHO \cdot (H_2O)_1$	−26.59	−24.98	−25.36
$CH_3COCH_3 \cdot (H_2O)_1$	−27.44	−25.68	−26.12

TABLE 3

Calculated spectral shifts (cm^{-1}) of $(H_2O)_1$-clusters for different basis sets

Cluster	Basis set		
	4-31G*	6-31G*	6-31G**
$CH_2O \cdot (H_2O)_1$	215	269	269
$CH_3CHO \cdot (H_2O)_1$	258	311	329
$CH_3COCH_3 \cdot (H_2O)_1$	158	188	190

with C_{LO} and C_{HO} as the LUMO and HOMO–MO coefficients at the O-atom.

The π–π^* excitation in *p*-cresol is connected with a charge transfer from the oxygen atom to the aromatic ring so that $q_0^* < q_0$, cf. the O-atom MO coefficients in Fig. 4. Hence for $+I$ effects with $\delta\alpha_0 > 0$, a red shift, $\Delta\delta E_\pi < 0$, is expected while for $-I$ with $\delta\alpha_0 < 0$ a blue shift, $\Delta\delta E_\pi > 0$, should result. This agrees with the ab initio calculations and the experimental results, if the first water molecule acts as electron donor and the second and third water molecules as electron acceptors. In phenol we again find that $q_0^* < q_0$ and the MO shifts are in the same directions as in Fig. 3, so that the argument for the observed red and blue shifts is analogous.

We believe that for π–π^* transitions in H-bonded clusters, the spectral shifts may quite generally originate from the inductive effect which the solvent molecule exerts on the solute chromophore. The question arises whether this scheme can also be applied to n–π^* transitions, e.g. in a carbonyl group.

Figure 4 shows the $CH_2O(H_2O)_1$ cluster configuration obtained from extensive geometry optimisation and basis sets, and procedures of different quality ranging from the simple STO-3G basis set to the second-order Møller–Plesset theory [6]. All calculations for the n–π^* transition are carried out with GAUSSIAN 90 on a Convex C 120 and the Møller–Plesset calculations on a Cray Y-MP at the KFA Jülich. Different conformations were tried with H_2O interacting with the H-atoms of CH_2O, forming a ring while interacting with the O-atom of the carbonyl group: a linear O···H–O configuration; an angled O···H–O configuration, and so on. For all these starting configurations we varied the C=O and O···H distances as well as the C=O···H, O···H–O and CH_2O···HOH (torsion) angles for energy optimisation. We find the configuration shown in Fig. 4 to be the most stable one with H_2O in the CH_2O plane, a C=O···H angle as expected from the oxygen lone pair orientation, and an O···HO angle substantially below 180° (possibly due to an O(H_2O)–H(CH_2O) interaction).

The best MP2 calculation gave r(C=O) = 1.21 Å, R(O···H) = 2.06 Å,

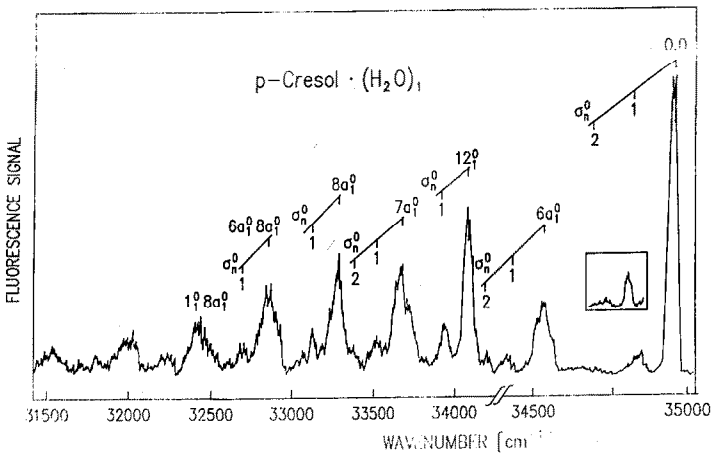

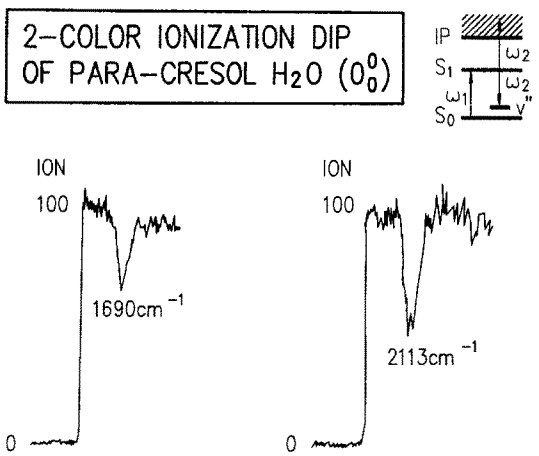

Fluorescence	Stimulated Emission	Assignment
1686cm^{-1}	1690	$8a_1^0$
2110	2113	$6a_1^0 8a_1^0$
2262	2260	2113+σ
2542	2540	$1_1^0 8a_1^0$

Fig. 5. (a) Dispersed fluorescence spectrum after excitation of (0,0) *p*-cresol · $(H_2O)_1$. The spectrum consists of progressions of the intermolecular stretch in the S_0 state σ_n and its combination bands with several intramolecular cluster vibrations. Frequency accuracy is ± 10 cm^{-1}. (b) Two-colour ionisation dip resonances after pumping the electronic origin of *p*-cresol · $(H_2O)_1$ with typical signals at 1690 cm^{-1} (8a) and 2113 cm (6a, 8a), leading to ion dips of up to 50%. Frequency accuracy is ± 1 cm^{-1}.

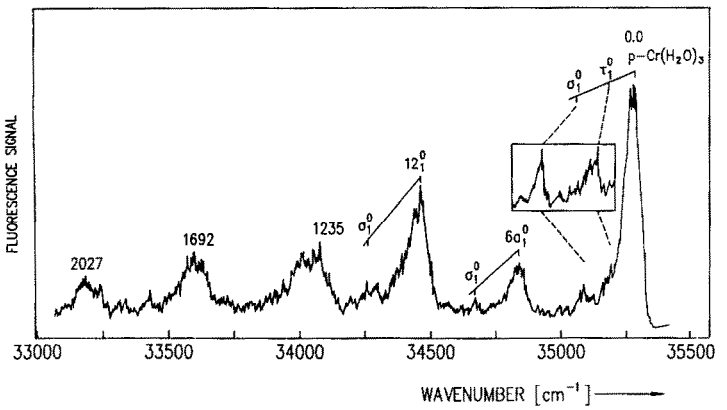

Fig. 6. Dispersed fluorescence spectrum after excitation of (0,0) *p*-cresol · $(H_2O)_3$. The spectrum consists of transitions from the vibrationless S_1 state to intermolecular cluster vibrations in the electronic ground state τ, σ and its combination bands with several intramolecular S_0-cluster vibrations.

$\angle(CO\cdots H) = 98.3°$, $\angle(O\cdots HO) = 145.12°$ and an H-bond energy of $-21.3\,kJ\,mol^{-1}$ (see Table 2).

In the $CH_2O(H_2O)_1$ cluster, the chromophore is the proton acceptor and we expect a negative (stabilising) $-I$ solvent effect. Indeed, both the *n*- and π^*-levels are stabilised by the H-bridge bond as shown in Fig. 4. The spectral shift depends on which molecular orbital is stabilised more strongly. This again depends on the O-atom charge order in the *n*- and π^*-levels of CH_2O, cf. eqns. (2) and (3).

It is well known that in carbonyl groups, the n–π^* transition is connected essentially with a charge transfer from the O-atom lone pair in the molecular plane to the carbon atom in a p-orbital perpendicular to that plane. This transition between two nearly perpendicular orbitals makes the n–π^* band forbidden and weak. For the $CH_2O(H_2O)_1$ and $CH_3COH(H_2O)_1$ systems all basis sets from STO-3G to 6-31G** show $C_{HO} > C_{LO}$ from which a stronger decrease of the *n*-orbital (HOMO), and thus a blue shift, results.

The spectral shifts after clustering are shown in Table 3 for the different basis sets used. The most stable configuration of the CH_3COH and CH_3COCH_3 clusters is similar to the $CH_2O(H_2O)_1$ case with non-linear $C{=}O\cdots H$ and $O\cdots H{-}O$ orientations, but with H_2O no longer in the chromophore plane.

To our knowledge there are as yet no experimental data on n–π^* transitions in H-bonded clusters of carbonyl chromophores. The electronic spectra of liquid acetone/H_2O show large blue shifts of around $2000\,cm^{-1}$. Supersonic jet spectroscopy of the CH_2O/H_2O system with a pick-up source and REMPI detection is under way.

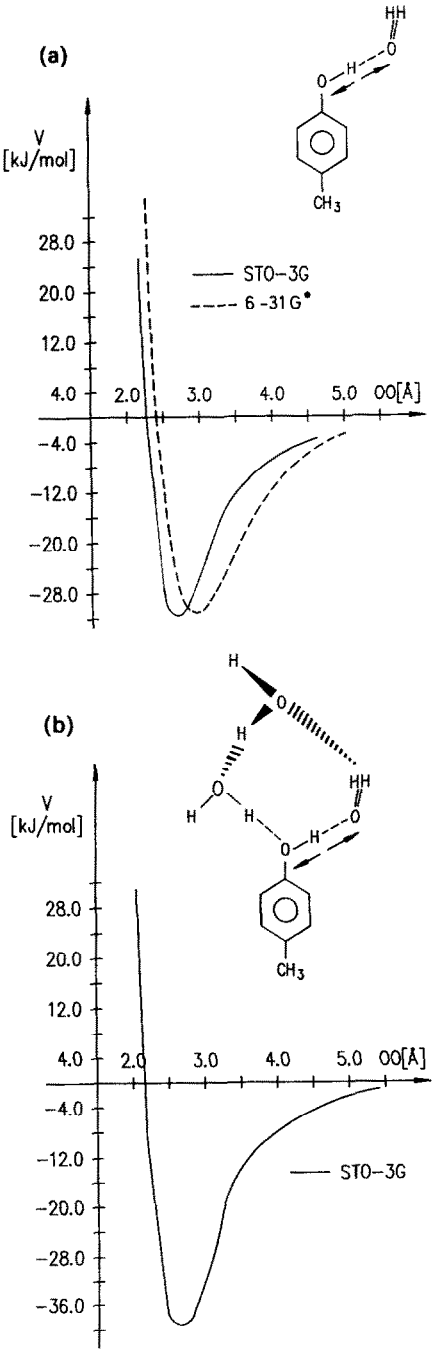

Fig. 7. Intermolecular stretch potentials of *p*-cresol · $(H_2O)_{1,3}$ obtained with different basis sets.

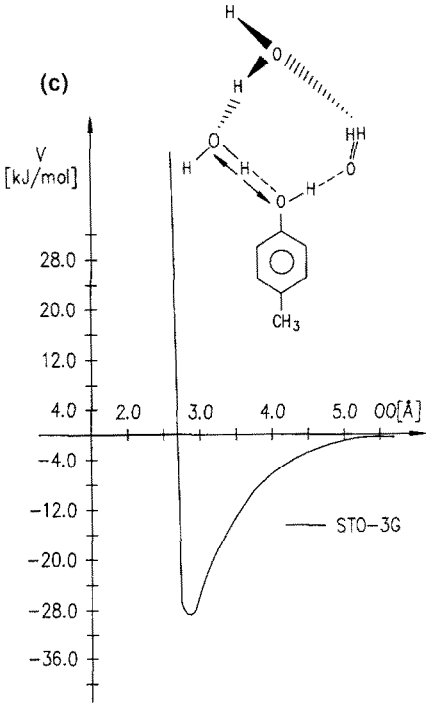

Fig. 7 continued.

Spectroscopy of intermolecular vibrations and comparison with theory

The dispersed fluorescence spectrum from excitation of (0,0) *p*-cresol · $(H_2O)_1$ shown in Fig. 5 indicates a slightly lower frequency for the stretching vibration in the electronic ground state than in the S_1 state. A progression with 146 cm^{-1} spacing can be observed, starting from the origin as well as from some intramolecular vibrations of the clusters and compared to 152 cm^{-1} in the S_1-state. Figure 5 shows typical two-colour ionisation dip signals after excitation of (0,0) *p*-cresol · $(H_2O)_1$ which can be associated with the corresponding bands in the dispersed emission spectrum. From the dip spectra, quite precise ground-state vibrational frequencies can be obtained with an accuracy of $\pm 1\,cm^{-1}$ compared with $\pm 10\,cm^{-1}$ in the dispersed emission spectra. Both methods yield a value of 146 cm^{-1} for the intermolecular stretch vibration. The red shift of *p*-cresol · $(H_2O)_1$ relative to *p*-cresol itself shows the H-bond to be stronger in the excited S_1 state than in the electronic ground state. Hence a higher stretch frequency in the S_1 state (152 cm^{-1}) compared with the S_0 state (146 cm^{-1}) is reasonable. The electronic ground-state data for the intermolecular stretch vibration can be compared with ab initio GAUSSIAN 80 calculations with a 4-31G* basis set,

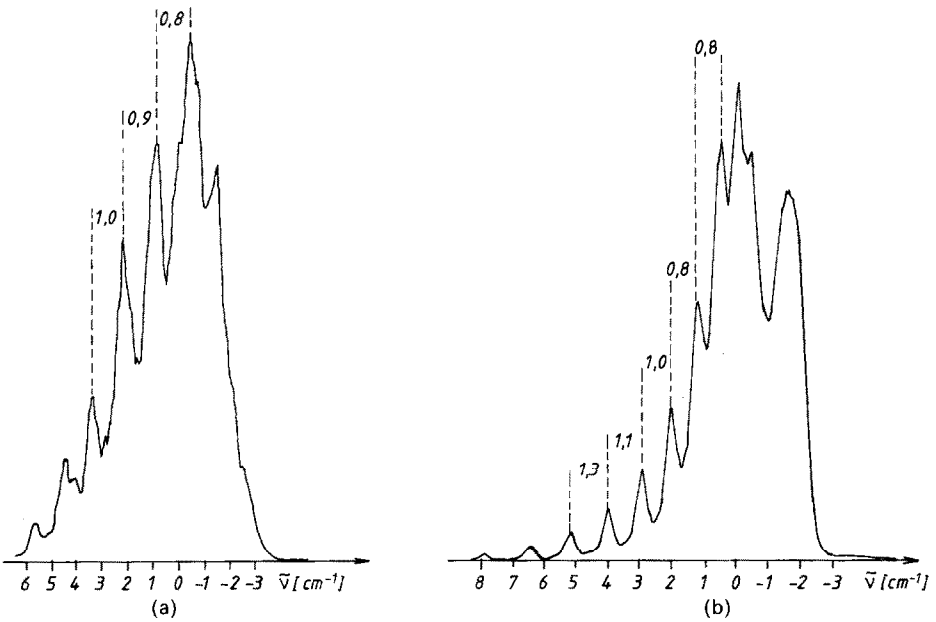

Fig. 8. (a) Experimental rotational contours of the *p*-cresol 1e″–2e′ band obtained with REMPI after $S_0 \rightarrow S_1$ excitation. (b) Simulated *p*-cresol 1e″–2e′ band. The simulation is described in the text.

where a stretch frequency of 175 cm^{-1} was obtained from the O–O potential curve of the translinear configuration of *p*-cresol · $(H_2O)_1$. The agreement with the experimental value of 146 cm^{-1} is reasonable. With a 6-31G* basis set we even obtained a stretch frequency of 154 cm^{-1}, in excellent agreement with experiment. As usual, the STO-3G potential is too rigid along the O–O-coordinate and leads to a stretch frequency of 234 cm^{-1} (see Fig. 7(a))).

There is a weak low-frequency feature in Fig. 1(b) at 122 cm^{-1} which is absent in the free *p*-cresol spectrum and hence cannot be ascribed to CH_3-rotation. From its low frequency and the C_s symmetry of *p*-cresol · $(H_2O)_1$, the band may stem from the totally symmetric (a′) in-plane bend vibration β', cf. the normal mode analysis of $(H_2O)_2$ in ref. 7.

Figure 6 shows the dispersed emission spectrum after excitation of (0,0) *p*-cresol · $(H_2O)_3$. Starting from the electronic origin of this cluster and from several intramolecular vibrations, a progression with a frequency of 185 cm^{-1} is observed which can be assigned to the intermolecular stretch vibrations. In the REMPI-spectrum in Fig. 1(d), we see a prominent band at 187 cm^{-1}, which is the corresponding intermolecular stretch vibration in the S_1 state.

It is quite interesting that the stretch frequency in the $n = 3$ cluster is considerably higher than in the $n = 1$ cluster. Figure 7(b) shows the corre-

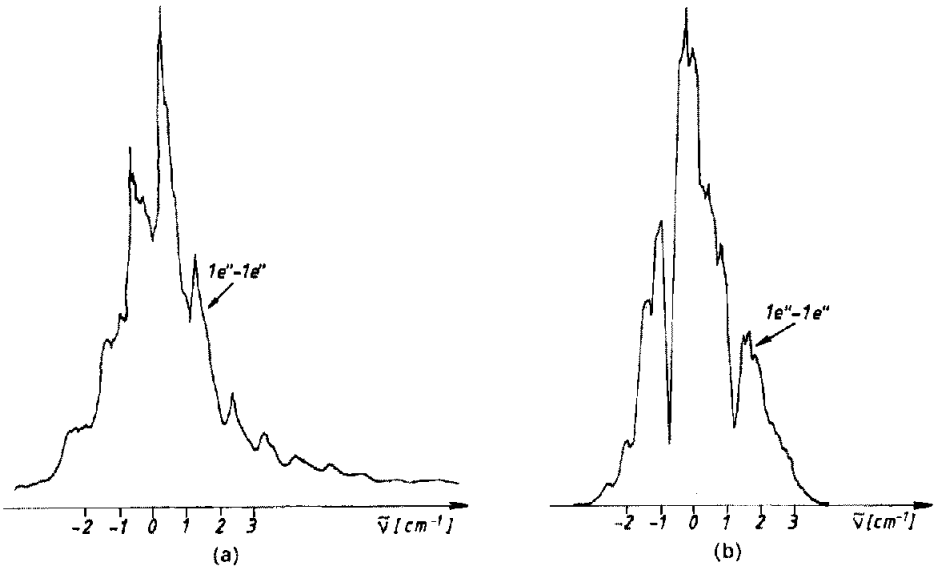

Fig. 9. (a) Experimental rotational contour of the *p*-cresol Oa_1'–Oa_1' band obtained with REMPI after $S_0 \rightarrow S_1$ excitation. Experimental conditions are 4 bar helium; $x/d = 500$; time base, 0.0017 nm min^{-1} (!). (b) Simulated Oa_1'–Oa_1' band with contribution from the 1e″–1e″ transition.

sponding cluster potential. The ab initio calculations show that the higher intermolecular stretch frequency (185 cm^{-1} compared to 146 cm^{-1}) arises from the more rigid O–O-potential of the cyclic $n = 3$ cluster. Figure 1(d) shows that the REMPI spectrum of *p*-cresol · $(H_2O)_3$ contains many low-

TABLE 4

Non-zero elements of the hamiltonian

Parameter	Value
Diagonals	
$\langle JK^{\pm}m^{\pm}\|H\|JK^{\mp}m^{\pm}\rangle$	$B + C/2[J(J+1) - K^2] + AK^2 + f(B-C)/4[J(J+1)]$
$\langle JK^{\pm}m^{\pm}\|H\|JK+2^{\pm}m^{\pm}\rangle$	$g \cdot (B-C)/4[(J-K)(J-K-1)(J+K+1)(J+K+2)]^{1/2}$
$\langle JK^{\pm}m^{\pm}\|H\|JK^{\mp}m^{\mp}\rangle$	$-2AKm$
f values	
$K^{\gamma} = 1^{+}$	1
$K^{\gamma} = 1^{-}$	−1
Other	0
g values	
$K > 0$	1
$K = 0$	$2^{1/2}$

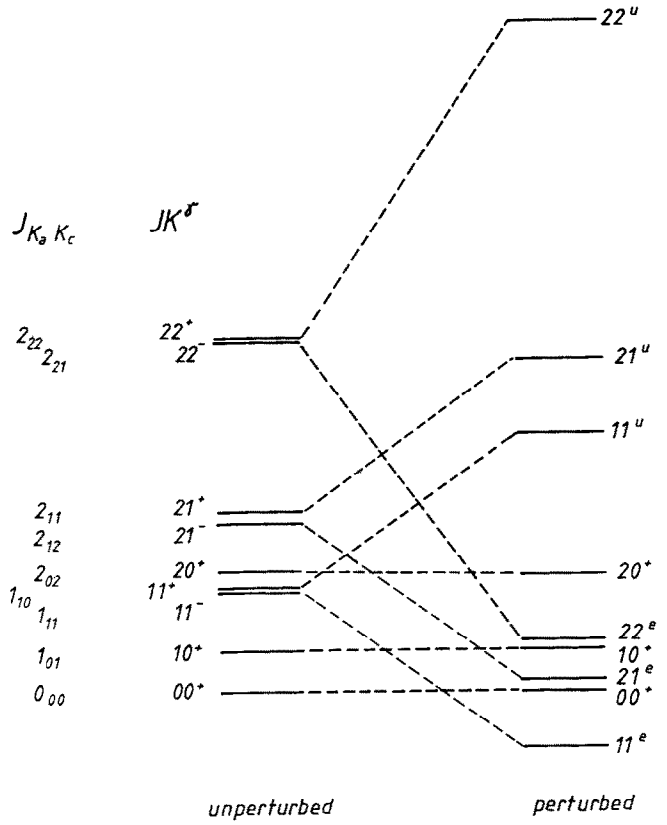

Fig. 10. Perturbation of asymmetric rotor levels by internal rotation up to $J = 2$.

frequency bands in addition to the usual intramolecular vibrational transitions, similar to *p*-cresol · $(CH_3OH)_1$. Furthermore, the dispersed emission spectra of *p*-cresol · $(H_2O)_3$ (Fig. 6) and *p*-cresol · $(CH_3OH)_1$ contain low-frequency bands not observed in *p*-cresol · $(H_2O)_{1,2}$. This can be attributed to the lowering of symmetry. While *p*-cresol · $(H_2O)_{1,2}$ still have C_s symmetry, i.e. the plane of the aromatic ring, *p*-cresol · $(H_2O)_3$ and *p*-cresol · $(CH_3OH)_1$ no longer have symmetry.

As shown in Fig. 6 and ref. 8, we observe bands at 74 and 70 cm^{-1} for *p*-cresol · $(H_2O)_3$ and *p*-cresol · $(CH_3OH)_1$ in the S_0 state and similar frequencies in the S_1 state. According to quantum chemical calculations of different groups on the translinear water dimer, there is only one vibrational band in the range 70–90 cm^{-1}. This band can be assigned to the torsional motion of the solvent molecule around the H-bridge axis and is named τ here.

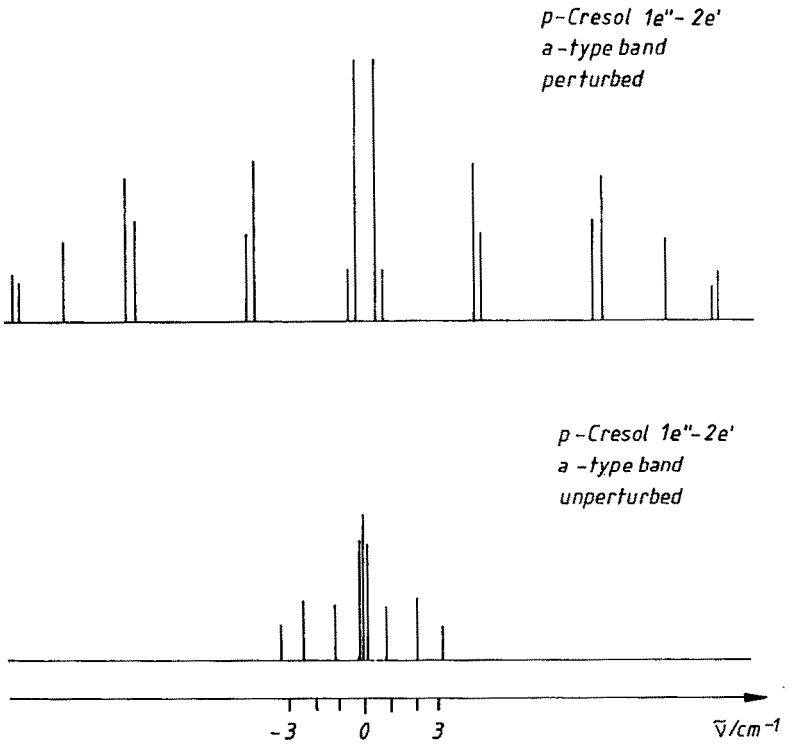

Fig. 11. Simulated broadening of torsional bands by perturbation with the overall rotation of the molecule.

CH_3-torsion/overall rotation-interaction in p-*cresol and* p-*cresol* · *$(H_2O)_1$*

While taking the REMPI spectra of *p*-cresol and *p*-cresol · $(H_2O)_1$ we observed that some of the CH_3-torsion bands were unusually broad and structured when taken with higher resolution, $< 0.2\,cm^{-1}$. Figure 8(a) shows the rotational structure of the 1e″–2e′-band with a $16\,cm^{-1}$ shift relative to the origin.

While the $0a_1'$–$0a_1'$ and 1e″–1e″ transitions follow type B selection rules, the electronically forbidden 1e″–2e′ transition, which is vibrationally induced and weak, follows type A selection rules. Here the direction of the transition moment and the axis of internal rotation coincide. Figure 9(a) shows the structure of the $0a_1'$–$0a_1'$ band which is superimposed by the 1e″–1e″ band system. The $0a_1'$–$0a_1'$ transition was simulated using an unperturbed asymmetric rotor model. The total band contour shown in Fig. 9(b) was simulated by superposition on the unperturbed 1e″–1e″ contour. Deviations are due to considerable perturbations of the 1e″–1e″ band by torsion–overall rotation interaction. The changes of rotational constants are

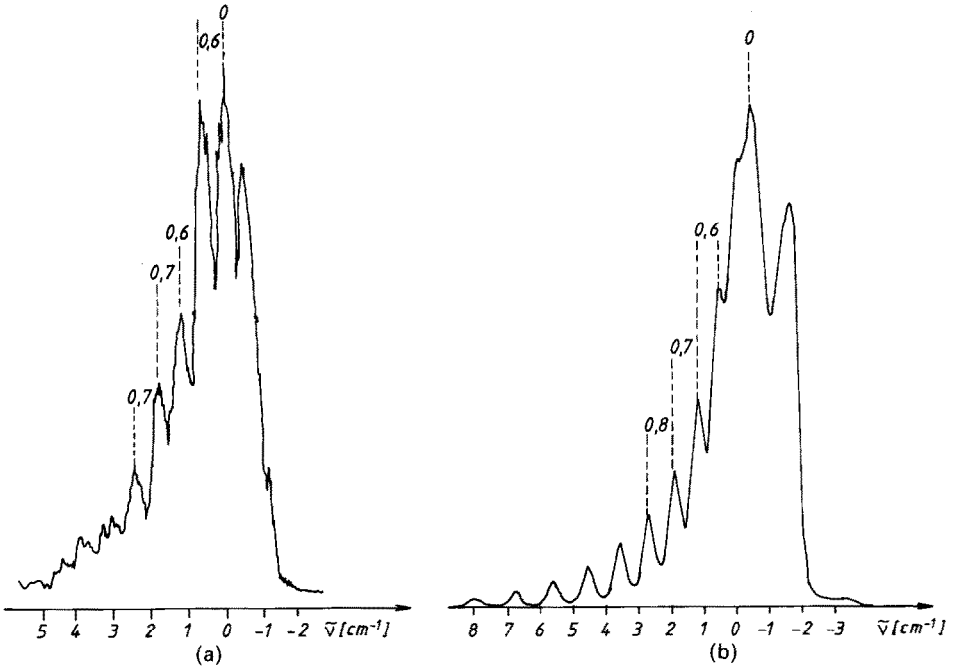

Fig. 12. (a) Experimental rotational contour of the *p*-cresol · $(H_2O)_1$ 1e″–2e′ CH_3 torsion band obtained with REMPI after $S_0 \rightarrow S_1$ excitation. Experimental conditions are 5 bar helium; 1 Torr H_2O; $x/d = 500$. (b) Simulation of the *p*-cresol · $(H_2O)_1$, 1e″–2e′ band. The simulation is described in the text.

$\Delta A = -0.0108\,cm^{-1}$, $\Delta B = 0.0006\,cm^{-1}$ and $\Delta C = 0.00016\,cm^{-1}$ based on a rotational temperature of 2 K.

Figure 8(a) shows the 1e″–2e′ band under the same expansion conditions as the electronic origin. Simulation of this band (Fig. 8(b)) was only possible with the assumption of a big change in the rotational constant A ($\Delta A = 0.0620\,cm^{-1}$). Such a considerable change is incompatible with the Franck–Condon principle, as the 0–0-band is the strongest transition. It can only be explained by coupling of the overall rotation of the molecule with the torsion of the methyl group. A rigid treatment of this problem can take this into account as a perturbation of the hamiltonian of the rigid rotor.

The quantum mechanical hamiltonian for this problem is

$$H = CJ_x^2 + BJ_y^2 + AJ_z^2 - AJ_zJ_\alpha + FJ_\alpha^2 + V(\Phi)$$

with $V(\Phi) = V_3/2\ (1 - \cos 3\Phi)$ as the threefold potential of the CH_3 hindered rotation; J the angular momentum operators for rotation around the three molecule axes and the internal rotation axis α; A, B, C the rotational constants and $F = \hbar^2 I_z/2I_\alpha(I_z - I_\alpha)$.

The basis functions are chosen as products of symmetric rotor [9] and

internal rotor wave functions [10]:

$$|JK\rangle|m^s\rangle = |JKm^s\rangle$$

Table 4 lists non-zero matrix elements of the hamiltonian [11]. The energy levels are obtained as usual by diagonalisation of the hamiltonian matrix. The relative intensity of the transition is given by

$$\text{rel.intensity} = \exp(-E''/kT)S^{v'\sigma'J'\tau'}_{v''\sigma''J''\tau''}$$

where E'' is the energy of the respective ground-state level. The line strength, $S^{v'\sigma'J'\tau'}_{v''\sigma''J''\tau''}$, of the transitions is

$$S^{v'\sigma'J'\tau'}_{v''\sigma''J''\tau''} = D^{J'}_{J}\left(\sum\sum c^{v'\sigma'J'\tau'}_{J'k'm^s'} c^{v''\sigma''J''\tau''}_{J''k''m^s''} G^{J'K'}_{J''K''}\right)^2$$

where c are coefficients of $|JK^\gamma m^s\rangle$ in the eigenvector of state $|v\sigma J\tau\rangle$.

The constants D and G can be shown to be [9]

P-lines: $D^{J-1}_{J} = (4J)^{-1}$

$$G^{J-K,K\pm1}_{J,K} = -2(J^2 - K^2)^{1/2}$$

Q-lines: $D^{J}_{J} = (2J+1)/[4J(J+1)]$

$$G^{J,J\pm1}_{J,K} = 2K$$

R-lines: $D^{J+1}_{J} = [4(J+1)]^{-1}$

$$G^{J+1,K\pm1}_{J,K} = 2[(J+1)^2 - K^2]^{1/2}$$

Figure 10 shows the perturbation of the asymmetric rotor levels by internal rotation up to $J = 2$ as calculated with this model. The notations for the energy levels are given in terms of symmetric rotor levels in the approximation of the prolate symmetric top (JK^γ) and also in the asymmetric rotor notation ($J_{K_aK_c}$). The perturbation increases with increasing rotational quantum number J, while levels with $K_a = 0$ in the asymmetric top notation remain unperturbed.

The principle broadening of a torsional band by perturbation from overall rotation is shown in Fig. 11, calculated up to $J = 2$. For a better quantitative agreement higher J have to be considered.

Because the perturbation increases with increasing torsional quantum number m of each vibronic level, the 1e″–2e′ transition is perturbed much more strongly than the 1e″–1e″ transition. In addition, in the 1e″–1e″ transition the perturbation nearly cancels because of equal torsional quantum numbers and similar rotational constants for both electronic states.

Figure 12(a) shows the 1e″–2e′ band of *p*-cresol · $(H_2O)_1$. Better expansion conditions were chosen in this experiment (backing pressure 5 bar, 0.94 Torr H_2O ($T = -18$°C) after a few days evacuation of the reservoir system),

because the heat of formation of the clusters at high H_2O densities will "warm up" the rotational temperature. It is evident that the spacing of the lines is smaller than in the case of the 1e″–2e′ band of the monomer. This is a consequence of the smaller rotational constants A, B and C compared with the monomer.

Figure 12(b) shows the simulated 1e″–2e′ band of *p*-cresol · $(H_2O)_1$. As in the case of the monomer, only a big change in ΔA yields satisfactory agreement with the experimental spectrum. A simulation based on a perturbation treatment as explained above will be published soon.

ACKNOWLEDGEMENTS

The authors thank the Deutsche Forschungsgemeinschaft and the European Community for financial support.

Thanks are due to Dr. J.M. Hollas for making available the asymmetric rotor contour program and to Professor R.D. Gordon for stimulating discussions.

REFERENCES

1 H.-H. Kuge and K. Kleinermanns, J. Chem. Phys., 90 (1989) 46.
2 U. Buck and H. Meyer, Phys. Rev. Lett., 52 (1984) 109.
3 K.H. Fung, H.L. Selzle and E.W. Schlag, Z. Naturforsch. Teil A, 36 (1981) 1338; Th. Weber and H.J. Neusser, J. Chem. Phys., 94 (1991) 7689.
4 K. Wolf, H.-H. Kuge and K. Kleinermanns, Z. Phys. D, 18 (1991) 409.
5 M. Pohl, M. Schmitt and K. Kleinermanns, J. Chem. Phys., 94 (1991) 1717.
6 C. Møller and M. Plesset, Phys. Rev., 46 (1934) 618.
7 J.R. Reimers and R.O. Watts, Chem. Phys., 85 (1984) 83.
8 M. Pohl, M. Schmitt and K. Kleinermanns, Chem. Phys. Lett., 177 (1991) 257.
9 H.C. Allen, Jr. and P.C. Cross, Molecular Vib-Rotors, Wiley, New York, 1963.
10 J.D. Lewis, T.B. Malloy, Jr., T.H. Chao and J. Laane, J. Mol. Struct., 12 (1972) 427.
11 R.D. Gordon, personal communication, 1991.